Probing the NADPH-binding site of *Escherichia coli* flavodoxin oxidoreductase

Claire LEADBEATER*, Lisa McIVER*, Dominic J. CAMPOPIANO*, Scott P. WEBSTER*, Robert L. BAXTER*, Sharon M. KELLY†, Nicholas C. PRICE†, Dominikus A. LYSEK*, Michael A. NOBLE*, Stephen K. CHAPMAN* and Andrew W. MUNRO‡[1]

*Department of Chemistry, Joseph Black Building, University of Edinburgh, The King's Buildings, West Mains Road, Edinburgh EH9 3JJ, U.K., †Department of Biological Sciences, University of Stirling, Stirling FK9 4LA, U.K., and ‡Department of Pure and Applied Chemistry, The University of Strathclyde, The Royal College, 204 George Street, Glasgow G1 1XL, U.K.

The structure of the *Escherichia coli* flavodoxin $NADP^+$ oxidoreductase (FLDR) places three arginines (R144, R174 and R184) in the proposed NADPH-binding site. Mutant enzymes produced by site-directed mutagenesis, in which each arginine was replaced by neutral alanine, were characterized. All mutants exhibited decreased NADPH-dependent cytochrome *c* reductase activity (R144A, 241.6 min^{-1}; R174A, 132.1 min^{-1}; R184A, 305.5 min^{-1} versus wild type, 338.9 min^{-1}) and increased K_m for NADPH (R144A, 5.3 μM; R174A, 20.2 μM; R184A, 54.4 μM versus wild type, 3.9 μM). The k_{cat} value for NADH-dependent cytochrome *c* reduction was increased for R174A (42.3 min^{-1}) and R184A (50.4 min^{-1}) compared with the wild type (33.0 min^{-1}), consistent with roles for R174 and R184 in discriminating between NADPH/NADH by interaction with the adenosine ribose 2′-phosphate. Stopped-flow studies indicated that affinity (K_d) for NADPH was markedly reduced in mutants R144A (635 μM) and R184A (2.3 mM) compared with the wild type (< 5 μM). Mutant R184A displays the greatest change in pyridine nucleotide preference, with the NADH/NADPH K_d ratio > 175-fold lower than for wild-type FLDR. The rate constant for hydride transfer from NADPH to flavin was lowest for R174A ($k_{red} = 8.82$ s^{-1} versus 22.63 s^{-1} for the wild type), which also exhibited tertiary structure perturbation, as evidenced by alterations in CD and fluorescence spectra. Molecular modelling indicated that movement of the C-terminal tryptophan (W248) of FLDR is necessary to permit close approach of the nicotinamide ring of NADPH to the flavin. The positions of NADPH phosphates in the modelled structure are consistent with the kinetic data, with R174 and R184 located close to the adenosine ribose 2′-phosphate group, and R144 likely to interact with the nicotinamide ribose 5′-phosphate group.

Key words: coenzyme affinity, enzyme kinetics, flavodoxin–$NADP^+$ oxidoreductase, protein engineering.

INTRODUCTION

The *Escherichia coli* flavodoxin–$NADP^+$ oxidoreductase (FLDR, or flavodoxin reductase, EC 1.18.1.2) is a 27.6 kDa FAD-containing enzyme which interacts with both *E. coli* flavodoxin (FLD) and ferredoxin redox partners and participates in a variety of important electron-transport systems in the bacterium; including the cobalamin-dependent methionine synthase and biotin synthase reactions [1,2]. In addition, the FLDR/FLD system is used to support the function of pyruvate-formate lyase and ribonucleotide reductase, which are key enzymes for the anaerobic growth of *E. coli* [3,4]. Interruption of the *fldr* gene in the *E. coli* chromosome is not lethal to the cells under normal growth conditions due to the presence of pyruvate–ferredoxin oxidoreductase, which can substitute for FLDR [5]. However, FLDR-knockout cells are particularly sensitive to oxidative stress. The *fldr* gene appears to be regulated by the *sox*RS regulon, since paraquat induces synthesis of FLDR [6]. Thus FLDR may be an important component of the cell's defence mechanism against reactive oxygen species. The physiological redox partner for FLDR is the FMN-containing FLD (19.6 kDa). The FLDR/FLD redox system has been shown to support activity of mammalian cytochromes P450 heterologously expressed in *E. coli*, and is thus of considerable biotechnological potential [7,8].

The recent solution of the atomic structure of FLDR (Protein Data Bank number 1FDR) [9] confirmed its structural similarity with other members of the ferredoxin reductase family of enzymes, including spinach ferredoxin–$NADP^+$ oxidoreductase (FNR) [10], corn nitrate reductase [11] and porcine cytochrome b_5 reductase [12]. The FLDR structure reveals an unusual flavin-binding conformation, with a hydrogen bond between the adenine and isoalloxazine rings, possibly explaining the unusual visible spectrum of the bound flavin [7]. It also reveals the presence of a distinct cleft adjacent to the isoalloxazine which is a likely docking site for flavodoxin, and which possibly involves the interaction of a series of positively charged arginines in a β-sheet segment of FLDR (R237, R238 and R239), with negatively charged glutamate and aspartate residues in the flavodoxin (E95, E127 and D134) [9]. The FLDR structure has also led to the suggestion that another cluster of arginine residues (R144, R174 and R184) is involved in the interaction with the pyridine dinucleotide cofactor (NADPH; Figure 1); although the cofactor was not co-crystallized with the enzyme [9]. In FLDR crystals, citrate precipitant was located bound in a site proposed to accommodate the adenine ribose of NADPH (based on homology with the spinach FNR) [9,10], and was seen to interact with amino acid R174, a conserved residue described as part of a 'fingerprint' region for $NADP^+$-binding members of the FNR-like family of flavoenzymes [13].

In recent potentiometric studies of FLDR, we have shown that the ligation of an NADPH analogue to the enzyme alters the driving force for electron transfer from the FAD enzyme, indicating that the binding of NADPH may regulate redox

Abbreviations used: FLD, *Escherichia coli* flavodoxin; FLDR, *Escherichia coli* flavodoxin–$NADP^+$ oxidoreductase; FNR, ferredoxin–$NADP^+$ oxidoreductase.

[1] To whom correspondence should be addressed (e-mail Andrew.Munro@strath.ac.uk).

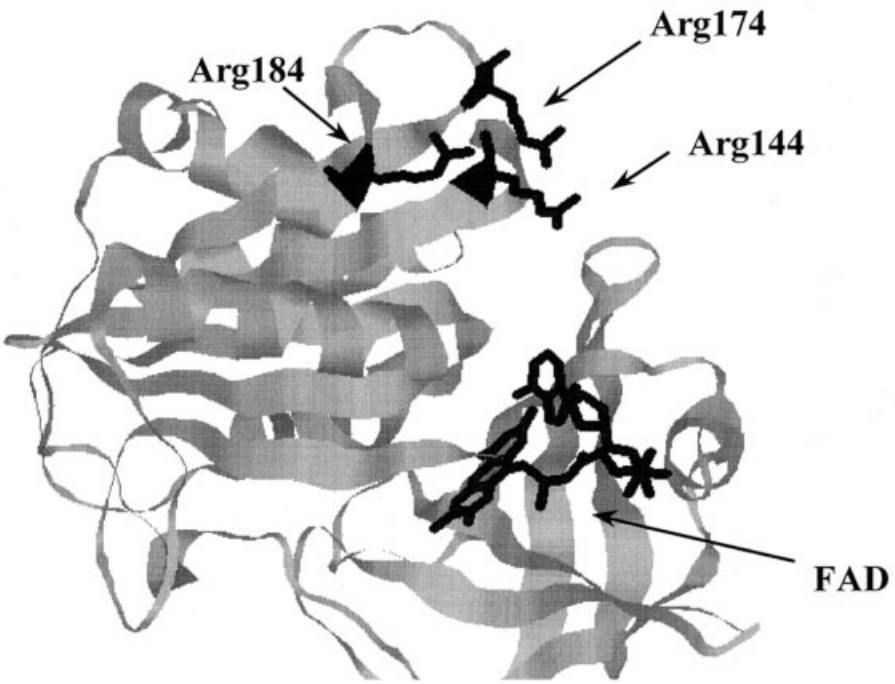

Figure 1 Ribbon diagram of the three-dimensional structure of FLDR (Protein Data Bank number 1FDR)

The positions of the three mutated arginine residues (R144, R174 and R184) are indicated in black, relative to the FAD moiety (also in black). The positively charged NH_2 groups of the arginines are exposed, providing potential interaction sites with the negatively charged phosphate groups of NADPH. The binding cavity for the NADPH cofactor lies between the arginines and the FAD.

properties of the flavin, as well as providing electrons for catalysis [7]. In this paper we report the characterization of R144A, R174A and R184A mutants of FLDR. These studies elucidate roles for these positively charged residues in the interaction with NADPH and in hydride transfer from the reduced pyridine dinucleotide to generate FAD hydroquinone on FLDR. We have determined the relative importance of each of these residues in the interaction with the pyridine nucleotide, and the distinct roles that each of these residues appears to play in the discrimination between NADPH/NADH and in overall catalysis of electron transfer from NAD(P)H to flavin and on to an electron acceptor (cytochrome *c*). Finally, we have used molecular modelling to dock NADPH with FLDR and examine the structural modifications required to enable suitable interaction of the coenzyme with the protein. Our results demonstrate that all three residues have important roles to play in the interaction with NADPH.

EXPERIMENTAL

E. coli strains and molecular biology

E. coli strain HMS174 (DE3) (F^-, *rec*A1, *hsd*R [r^-_{K12} m^+_{K12}] Rif^r[DE3]) [14] was used for overexpression of the *fldr* gene. Plasmid pCL21 (a derivative of pET 16b, Novagen, Madison, WI, U.S.A.) was used for production of FLDR and was constructed by PCR amplification of the structural gene from plasmid pEE1010 (a gift from Dr Elizabeth Haggård-Ljungquist, Department of Chemistry, Karolinska Institute, Stockholm, Sweden), as previously reported [7,15]. The wild-type *fldr* gene was expressed under the control of an isopropyl β-D-thiogalactoside-inducible T7 promoter in pCL21. For the generation of mutants R144A, R174A and R184A, the *fldr* gene was subcloned into pUC18 [16] using the *Nco*I and *Bam*HI restriction sites.

Site-directed mutagenesis was performed using the 'megaprimer' PCR method [17] using vector forward (5′-CGCCAGGGTTTTCCCAGTCACG-3′) and reverse (5′-GTTGTGTGGAATTGTGAGCGG-3′) oligonucleotides, and the following mutagenic primers: R144A, 5′-CACGCGGCCGCCTATGCCGCCGAC-3′; R174A, 5′-GTGGTCAGTGCAGAAACGGCAGCG-3′ and R184A, 5′-CTCACCGGCGCCATACCGGCATTA-3′, where the underlined bases indicate the position at which an arginine codon is replaced by one encoding alanine. Mutated *fldr* genes were digested with *Nco*I and *Bam*HI and re-cloned into pUC18 [16]. The *E. coli* strain TOP10 One Shot™ (F^-, *mcr*A, Δ[*mrr*$^-$ *hsd*RMS-*mcr*BC], Φ80*lac*ZM15, Δ*lac*X74, *deo*R, *rec*A1, *ara*D139, Δ[*ara-leu*]7697, *ga*/U, *ga*/K, *rps*L, *end*A1, *nup*G; Invitrogen) was used for transformation of the mutant ligation mixes in order to optimize the efficiency of mutant isolation. Mutant sequences were verified by the Sanger dideoxy chain-termination method. Protein expression was in *E. coli* strain C6007, which is deficient in the host *fldr* gene [5].

Enzyme preparations

Wild-type FLDR [from HMS174 (DE3)/pCL21] and mutant (from C6007/pCL22-24) forms were prepared from cultures grown in 2–10 litres of Luria–Bertani medium containing ampicillin (100 μg/ml). Transformant cells [C6007/pCL22 (R144A), pCL23 (R174A) and pCL24 (R184A)] were induced with 1 mM isopropyl β-D-thiogalactoside at an A_{600} of 1.0 and harvested after a further 3 h at 37 °C. The cells ($\approx$ 25 g of wet weight/l) were then pelletted by centrifugation (5000 ***g*** for 20 min at 4 °C), washed by resuspension in ice-cold buffer A (10 mM sodium phosphate, pH 7.5) and lysed by intermittent sonication (30 s on, 30 s off) for 5 min. Cellular debris was removed by centrifugation (15000 ***g*** for 30 min at 4 °C) and the supernatant was loaded

directly on to a Q-Sepharose 26/10 Hi-Load anion-exchange column (Pharmacia) that had been pre-washed in buffer A. Protein was eluted with a gradient (0–1 M) of NaCl in buffer A. Yellow FLDR-containing fractions were collected from 130 to 150 mM NaCl, combined and loaded on a 2′,5′-ADP–Sepharose column (1 cm × 20 cm) pre-equilibrated with buffer A containing 150 mM NaCl. Pure FLDR was eluted using buffer A containing 500 mM NaCl. The purified enzymes were dialysed against buffer A, concentrated by ultrafiltration (Amicon, 10000 Da cut-off) to a concentration of ≈ 5 mg/ml and stored frozen at −20 °C. PMSF (0.1 mM) was added to all buffers to minimize proteolysis. The purity and integrity of wild-type and mutant FLDR forms were assessed by SDS/PAGE.

Enzyme assays

Steady-state kinetic parameters for wild-type and mutant forms of FLDR were measured at 30 °C in 10 mM sodium phosphate (pH 7.5; assay buffer) on a Shimadzu 2101 UV-visible spectrophotometer. Reduction of cytochrome *c* (horse heart, type I) was monitored by absorbance increase at 550 nm, using an absorbance coefficient ($\Delta\epsilon_{red\text{-}ox}$) of 22640 $M^{-1}\cdot cm^{-1}$.

Stopped-flow measurements of transient absorbance changes associated with reduction of FLDR flavin (decrease in absorbance at 456 nm) and reduction of cytochrome *c* (550 nm) were made using an Applied Photophysics SF.17 MV stopped-flow spectrophotometer. Reactions were performed at 30 °C in assay buffer (pH 7.5) unless otherwise stated. Data analysis was performed using the SF.17 MV software and Origin (Microcal), both of which use non-linear least-squares regression analysis. The reduction of wild-type and mutant forms of FLDR by NADPH and NADH were measured at 456 nm (total flavin reduction) by rapid mixing of NAD(P)H (100 μM–10 mM) with enzyme (10–40 μM).

MS

Electrospray ionization MS was performed on a Micromass platform quadrupole mass spectrometer equipped with an electrospray ion source. The cone voltage was set to 70 V and the source temperature to 65 °C. A Waters 2690 HPLC unit with a Waters 486 tunable absorbance detector was connected to the mass spectrometer. Protein samples (10 μg of protein in 10 mM sodium phosphate, pH 7.5) were separated on a Jupiter 5 μg C-4 300A column at a constant trifluoroacetic acid concentration of 0.01 % using a linear gradient of 10–100 % acetonitrile in water over 40 min, at a flow rate of 0.05 ml/min. The total ion count of all ions in the m/z range 500–2000 and the UV chromatogram at 280 nm were recorded for the reversed-phase HPLC separation. The mass spectrometer was scanned at intervals of 0.1 s, the scans accumulated, the spectra combined and the average molecular mass determined using the MaxEnt and Transform algorithms of MassLynx software.

Spectroscopic characterization

Wild-type and mutant FLDR proteins were analysed by UV-visible spectrophotometry, CD and fluorescence spectroscopy. Protein samples were in assay buffer (10 mM sodium phosphate, pH 7.5) throughout. All UV-visible spectra were run on a Shimadzu 2101 scanning spectrophotometer. CD measurements were made in the far-UV (190–260 nm), near-UV (260–320 nm) and visible (320–600 nm) regions on a Jasco J-600 spectropolarimeter at protein concentrations of ≈ 15–20 μM (far UV) and ≈ 30–80 μM (near UV-visible). Aromatic amino acid fluorescence was measured on a Shimadzu RF-5301 spectrofluorophotometer with the excitation wavelength set at 290 nm and emission measured between 300 and 400 nm, using ≈ 0.5 μM protein. Flavin fluorescence was measured with excitation at 456 nm and emission at 500–600 nm, also using ≈ 0.5 μM protein. Excitation and emission slit widths on the Shimadzu instrument were set at 5 nm/5 nm for tryptophan fluorescence, and at 10 nm/10 nm for flavin fluorescence.

Molecular modelling and sequence alignments

Atomic co-ordinates for protein were taken from the 1.7 Å-resolution X-ray structure of FLDR (Protein Data Bank number 1FDR) [9]. All modelling studies were carried out using residues 2–248, excluding residues 44–46, which could not be refined in the original structure. The graphics program SYBYL (Tripos) was used to dock the NADPH on to FLDR, and to rotate W248. The restraints for this preliminary model were that the hydride–isoalloxazine distance should be less than 8 Å and residues R144, R174 and R184 should be close to, or form part of, the intermolecular recognition surface.

A number of possible orientations were selected as starting points for further molecular mechanics refinement to remove any short non-bonded contacts and to optimize any intermolecular hydrogen bonds and salt bridges using the program Biopolymer-flexidock within SYBYL, allowing a maximum of 3000 generations. All non-hydrogen atom positions of the amino acid residues and prosthetic groups in FLDR and NADPH were refined using a Powel least-squares minimization algorithm with the standard geometry definitions. No water or other solvent molecules were included in any of the models.

Amino acid sequence alignments of FLDR with other proteins were performed using the MSA (Multiple Sequence Alignment) program from Washington University.

RESULTS

Protein expression and purification

Wild-type and mutant FLDRs were overexpressed successfully in *E. coli* and purified to homogeneity in two chromatographic steps (Q-Sepharose and 2′,5′-ADP–Sepharose). The expression of mutant forms from plasmids pCL22-24 under the *lac* promoter system in the background of strain C6007 (*fldr*$^-$) was not as high

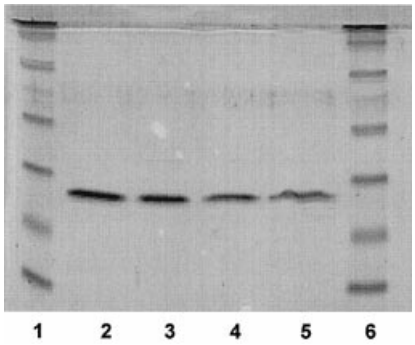

Figure 2 SDS/PAGE of purified wild-type and mutant (R144A, R174A and R184A) forms of FLDR

Lane 1, molecular-mass standards (94000, 67000, 43000, 30000, 20100 and 14400 Da); lane 2, wild-type FLDR; lane 3, R144A FLDR; lane 4, R174A FLDR; lane 5, R184A FLDR; lane 6, as lane 1.

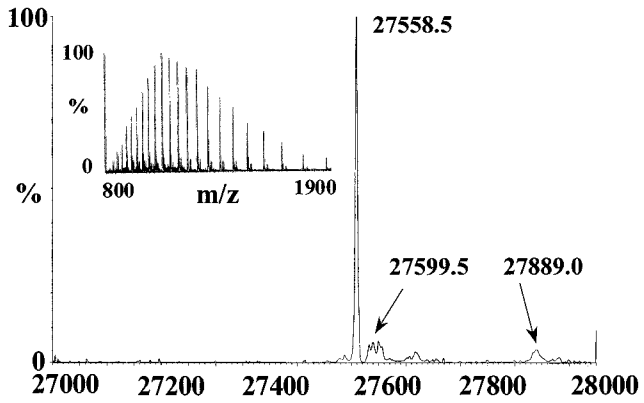

Figure 3 Typical electrospray ionization MS spectrum of a purified FLDR enzyme

The mass spectrum shown is that of mutant R174A. Conditions were as described in the Experimental section: 10 μg of pure R174A mutant in 10 mM sodium phosphate (pH 7.5) was used for the procedure. The inset shows the total ion count of all ions in the *m/z* range 500–2000 (peaks at 785.3, 788.4, 811.7, 836.2, 862.2, 890.1, 919.7, 951.2, 985.2, 1021.7, 1060.9, 1103.3, 1149.3, 1199.3, 1253.7, 1268.7, 1313.3, 1329.2, 1379.0, 1395.5, 1451.4, 1468.5, 1532.1, 1550.2, 1622.0, 1641.5, 1723.3, 1744.1, 1838.3 and 1969.3). The main diagram shows the sum of accumulated scans, giving rise to the molecular mass of FLDR mutant R174A (27558.5 Da).

($\geqslant$ 2 mg of pure enzyme/litre of cells) as that obtained for the wild-type under the T7 promoter from plasmid pCL21 ($\geqslant$ 30 mg of pure FLDR/litre [7]), necessitating purification from a larger *E. coli* transformant cell mass (10–20 litres versus 2 litres for wild-type FLDR). However, the use of strain C6007 guaranteed lack of contamination with the wild-type FLDR, which is expressed naturally at high levels. Wild-type and mutant forms of FLDR proved very insensitive to proteolysis in the homologous host organism, as can be seen by SDS/PAGE (Figure 2). The stability of the FLDR proteins also enabled the collection of high-resolution mass spectrometric data (Figure 3), confirming the isolation of homogeneous, non-proteolysed protein.

Spectroscopic characterization

UV-visible spectrophotometry

The wild-type and mutant FLDRs had essentially identical visible absorption spectral characteristics, with absorbance maxima at 456 and 400 nm, and a shoulder on the longer-wavelength band at 483 nm (Figure 4, left-hand panel). The far-UV absorption maxima were at 280 nm for all forms. The ratio of absorbance at 280 nm/456 nm (protein/flavin) was 6.5 ± 0.2 for pure wild-type FLDR and the mutants. Occasional mutant preparations had slightly higher protein/flavin ratios, due to lower flavin content. However, preparations always contained $> 85\%$ holoenzyme and those used for kinetic studies contained $> 95\%$ flavin. Preparations of purified mutant and wild-type FLDRs were quantified using a molar absorption coefficient of 7100 $M^{-1} \cdot cm^{-1}$ at 456 nm [8].

CD spectroscopy

The wild-type and mutant FLDRs had very similar far-UV CD spectra, exhibiting a negative Cotton effect from 202 to $\approx$ 250 nm, and positive ellipticity at wavelengths from 202 to 190 nm. The minimum was at $\approx$ 215 nm for all FLDRs. The visible CD spectra of the proteins were also very similar, showing positive ellipticity in the region of the first flavin visible absorption band (385 nm) with a peak at 388 nm and a less intense band of negative ellipticity in the region of the second flavin visible band (456 nm), centred at 454 nm (Figure 4, right-hand panel). In the near-UV region, all FLDRs exhibited a very strong, sharp signal of positive ellipticity, centred at 272 nm. The intensity of the signal indicates that it may derive from stacking interactions between the FAD and one or more aromatic residues in FLDR. The R144A and R184A mutations did not alter significantly the intensity or position of this near-UV band. However, the intensity (but not position) of the band appears slightly lower in mutant R174A (Figure 4, right-hand panel), which also exhibits unusual aromatic amino acid fluorescence properties (see below).

Fluorescence spectroscopy

The fluorescence properties of wild-type and mutant FLDRs were compared to provide further information on tertiary

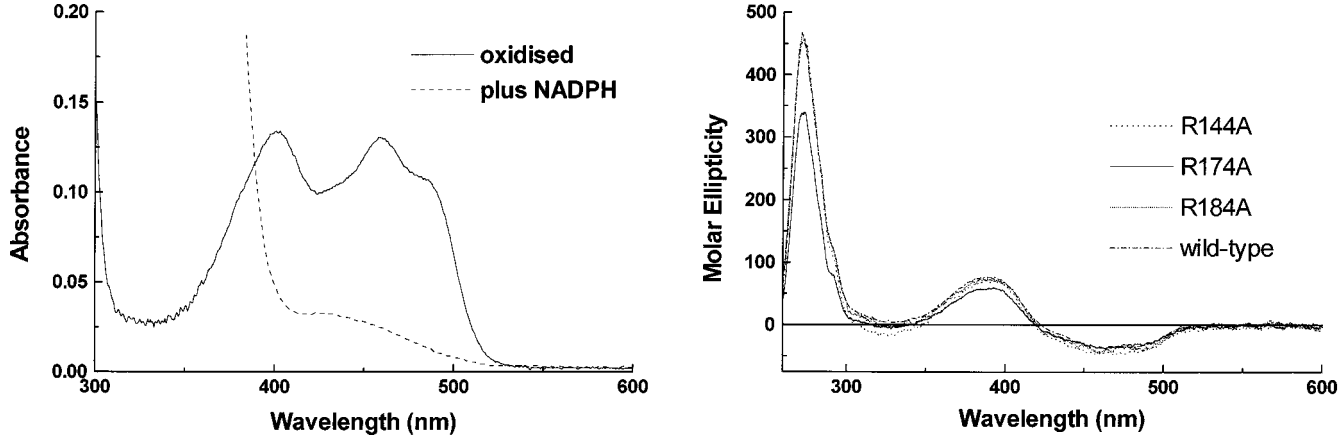

Figure 4 Spectral properties of wild-type and mutant FLDR proteins

(Left-hand panel) Visible absorption spectrum of oxidized FLDR mutant R144A (18 μM; solid line). The protein was reduced to its hydroquinone form by addition of 100 μM NADPH (dashed line). The spectra were measured on a Shimadzu 2101 UV-visible scanning spectrophotometer, as described in the Experimental section. (Right-hand panel) Near-UV-visible CD spectra of wild-type and mutant forms of FLDR. All proteins were at a final concentration of 70 μM in buffer A. Spectra were measured between 600 and 260 nm on a Jasco J-600 spectropolarimeter, as described in the Experimental section.

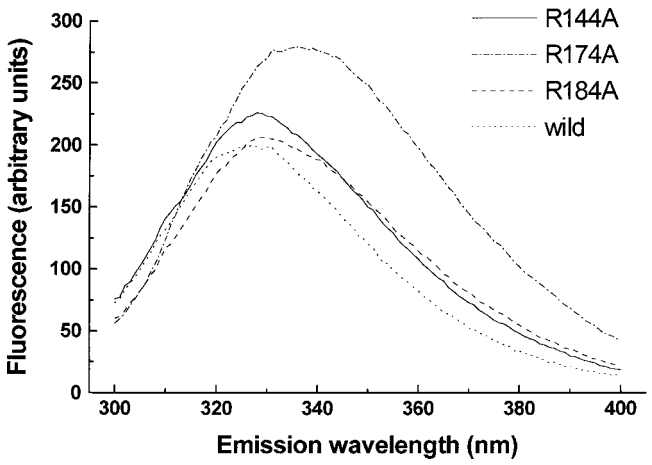

Figure 5 Aromatic fluorescence spectra from wild-type and mutant (R144A, R174A and R184A) FLDRs

Fluorescence spectra were measured on a Shimadzu RF-5301 spectrofluorophotometer with the excitation wavelength set at 290 nm and emission measured between 300 and 400 nm, as described in the Experimental section. Protein concentrations were 0.45 μM (wild-type FLDR), 0.48 μM (R144A), 0.45 μM (R174A) and 0.45 μM (R184A).

structure (aromatic amino acid fluorescence) and flavin environment (flavin fluorescence). Flavin emission (excitation 456 nm, emission 500–600 nm) from all FLDRs was low, due to strong quenching of the chromophore by the surrounding protein matrix. By comparison of the fluorescence of the FLDRs with that of free FAD under the same conditions, and with the knowledge of the quantum yield (Q_f) for FAD (0.032) [18], the Q_f values for the FLDR-bound flavins were all measured to be < 0.001, i.e. negligible fluorescence. Using high flavoprotein concentrations ($\approx 0.5\ \mu$M) and wide slit widths (10 nm/10 nm excitation/emission on the Shimadzu instrument) the flavin emission maxima were found to be at 528 nm for wild-type and mutant FLDRs. As expected, disruption of the protein structure with the denaturant guanidinium chloride led to large increases in the flavin fluorescence (results not shown).

Aromatic amino acid (primarily tryptophan) fluorescence (excitation 290 nm, emission 300–400 nm) was measured for wild-type and mutant FLDRs (0.05 μM) with excitation/emission slit widths set at 5 nm on the Shimadzu instrument. Emission spectra were of similar intensity and had similar emission maximum (328 nm) for wild-type and for R144A and R184A FLDRs. However, the emission from mutant R174A was of slightly greater intensity and was maximal at a longer wavelength (336 nm; Figure 5).

Steady-state kinetics

In a previous publication [7], we reported a k_{cat} of 141.3 min^{-1} for cytochrome *c* reduction by wild-type FLDR in 100 mM sodium phosphate (pH 7.5). However, we established in the current study that interaction with the cytochrome was primarily electrostatic and was enhanced at lower ionic strength, being optimal at 10 mM sodium phosphate (pH 7.5; assay buffer). The steady-state kinetic behaviour of wild-type and mutant FLDR enzymes was re-investigated in the lower-ionic-strength assay buffer using either NADPH or NADH as the donor. Preliminary experiments indicated that the K_m value for NADPH was $\approx 4\ \mu$M [7] and for NADH was ≈ 2 mM. A set of experiments was performed with NADPH/NADH at saturating or near-saturating conditions (200 μM and 10 mM, respectively) and cytochrome *c* varied between 0 and 100 μM. With NADPH as the donor, wild-type FLDR catalysed cytochrome *c* reduction with a k_{cat} of $338.9 \pm 7.2\ min^{-1}$ and a K_m of $17.6 \pm 1.6\ \mu$M for cytochrome *c*. The k_{cat} values were lower for all mutants (Table 1). With NADH as the donor, all k_{cat} values were much lower relative to NADPH (Table 1). The apparent K_m values for cytochrome *c* were also markedly decreased ($3.2 \pm 0.19\ \mu$M for the wild type, $0.82 \pm 0.04\ \mu$M for mutant R144A, $5.9 \pm 0.46\ \mu$M for R174A and $4.4 \pm 0.35\ \mu$M for R184A), although this may only indicate that cytochrome *c* is able to saturate the FLDR at much lower concentrations with the less-efficient NADH as the reductant. However, the k_{cat} values for mutants R174A and R184A with NADH were both higher than that for the wild type, whereas R144A had a lower k_{cat} value (Table 1).

With cytochrome *c* maintained at a saturating concentration (200 μM), the K_m values for NAD(P)H were also determined by steady-state kinetic analysis. As expected, wild-type FLDR had a lower K_m for NADPH ($3.9 \pm 0.3\ \mu$M) than any of the mutants. In particular, R184A had a K_m of $54.4 \pm 5.9\ \mu$M for NADPH, > 14 times that for wild-type FLDR (Table 1). The K_m for NADH was also much greater for mutants R144A (5.14 ± 0.51 mM) and R174A (9.86 ± 0.79 mM) than for wild-type FLDR (2.04 ± 0.17 mM). The NADH affinity of mutant R184A was the same (within the limits of error) as that of wild-type FLDR (K_m, $1.66 \pm 0.22\ \mu$M; Table 1).

Stopped-flow kinetics

Stopped-flow absorption spectrophotometry was used to investigate the effects of mutations on the microscopic rate constants for the NAD(P)H-dependent flavin-reduction step in the catalytic cycle.

Table 1 Steady-state kinetic parameters for cytochrome *c* reduction with NAD(P)H by wild-type and mutant (R144A, R174A and R184A) forms of FLDR, measured at 550 nm

Reactions were performed at 30 °C in assay buffer, as described in the Experimental section.

	K_m		k_{cat}		k_{cat}/K_m	
	NADPH (μM)	NADH (mM)	NADPH (min^{-1})	NADH (min^{-1})	NADPH ($\mu M^{-1} \cdot min^{-1}$)	NADH ($mM^{-1} \cdot min^{-1}$)
Wild type	3.9 ± 0.3	2.04 ± 0.17	338.9 ± 7.2	33.0 ± 0.4	86.9 ± 9.2	16.2 ± 1.6
R144A	5.3 ± 0.7	5.14 ± 0.51	241.6 ± 6.1	13.7 ± 0.1	45.7 ± 8.2	2.67 ± 0.31
R174A	20.2 ± 0.9	9.86 ± 0.79	132.1 ± 4.2	42.3 ± 1.4	6.5 ± 0.5	4.29 ± 0.53
R184A	54.4 ± 5.9	1.66 ± 0.22	305.5 ± 6.9	50.4 ± 1.1	5.6 ± 0.9	30.4 ± 5.4

Table 2 Stopped-flow kinetic parameters for NAD(P)H-dependent flavin reduction in wild-type and mutant (R144A, R174A and R184A) forms of FLDR, measured at 456 nm

Reactions were performed at 30 °C in assay buffer, as described in the Experimental section.

	K_d		k_{red}		k_{red}/K_d	
	NADPH (μM)	NADH (mM)	NADPH (s^{-1})	NADH (s^{-1})	NADPH ($\mu M^{-1} \cdot s^{-1}$)	NADH ($mM^{-1} \cdot s^{-1}$)
Wild type	< 5	1.67 ± 0.38	22.63 ± 0.67	7.79 ± 0.61	4.53 ± 0.13	4.66 ± 1.09
R144A	635 ± 10	56.15 ± 4.55	12.94 ± 0.73	10.09 ± 0.61	0.0204 ± 0.0015	0.18 ± 0.03
R174A	< 5	4.14 ± 0.49	8.82 ± 0.52	9.05 ± 0.47	1.76 ± 0.11	2.18 ± 0.43
R184A	2300 ± 60	4.35 ± 0.6	15.22 ± 0.14	4.24 ± 0.39	0.00667 ± 0.00019	0.97 ± 0.26

NADPH

For wild-type FLDR (34 μM), negligible variation in the rate of NADPH-dependent reduction (k_{red}) was seen between 100 μM and 10 mM reductant. FLDR was reduced with a rate constant of $22.63 \pm 0.67\ s^{-1}$ and the K_d was $< 5\ \mu$M. A similar phenomenon ($K_d < 5\ \mu$M) was observed with mutant R174A, with the flavin-reduction rate constant over the entire NADPH concentration range. However, for R174A the value of k_{red} was considerably lower than for the wild type ($8.82 \pm 0.52\ s^{-1}$). For mutants R144A and R184A, a clear flavin-reduction rate-dependence on [NADPH] was observed. A plot of reduction rate versus [NADPH] described a rectangular hyperbola, from which a K_d and k_{red} could be determined. The apparent affinity for NADPH was dramatically weakened in both R144A (K_d, $635 \pm 10\ \mu$M) and R184A (K_d, 2.3 ± 0.06 mM), although the k_{red} values were not lowered to the same extent (R144A, $12.94 \pm 0.73\ s^{-1}$; R184A, $15.22 \pm 0.14\ s^{-1}$). The k_{red}/K_d ratio for each enzyme indicates the relative efficiency of the NADPH-binding and flavin-reduction process. The ratios for R144A and R184A were markedly (> 220-fold and > 670-fold, respectively) lower than those for wild-type FLDR (Table 2).

NADH

The affinity of wild-type and mutant FLDRs for NADH was considerably lower than that for NADPH. The rate of flavin reduction showed a clear [NADH]-dependence for all enzymes, allowing calculation of k_{red} and K_d by fitting data points to the Michaelis function. Wild-type FLDR had the highest apparent affinity for NADH (K_d, 1.67 ± 0.38 mM), while R144A had the lowest (K_d, 56.15 ± 4.55 mM). R174A and R184A had apparent affinities ≈ 2.5-fold lower than wild-type FLDR (Table 2). Less variation was observed for the k_{red} values, with both R144A ($10.09 \pm 0.61\ s^{-1}$) and R174A ($9.05 \pm 0.47\ s^{-1}$) giving higher rates than the wild type ($7.79 \pm 0.61\ s^{-1}$). The k_{red}/K_d ratio for wild-type FLDR ($4.66 \pm 1.09\ mM^{-1} \cdot s^{-1}$) was the highest, with R144A having the lowest value (k_{red}/K_d, $0.18 \pm 0.03\ mM^{-1} \cdot s^{-1}$) (Table 2).

DISCUSSION

In their report of the atomic structure of the FLDR, Ingelman et al. [9] identified arginines 144, 174 and 184 as putative components of the NADPH-binding site of the enzyme; although this site was occupied by citrate in the crystal structure. Examination of the structure highlights this cluster of three positively charged arginine residues located at the cleft between the NADP(H)-binding and FAD-binding sub-domains of the enzyme (Figure 1). We expected to find that one or more of the arginines would play key roles in the recognition of pyridine dinucleotide and/or the distinction between NADPH/NADH (which differ only in the presence of a phosphate group, rather than a hydroxy, at the 2′ position of the pyridine moiety). The results of steady-state kinetic studies on R144A, R174A and R184A mutants (Table 1) indicate that the removal of the positively charged arginine at each of these positions causes decreased NADPH-dependent cytochrome *c* reductase activity. In addition, stopped-flow studies show that each mutation has clear effects on the binding of NADPH and/or the process of hydride transfer to the flavin (Table 2). Thus kinetic data indicate that all three arginines have major roles in FLDR catalysis. In terms of the severity of the overall effects of these mutations, R174 and R184 appear much more important for NADPH-dependent activity than does R144. From steady-state studies, the k_{cat}/K_m ratio for R174A and R184A (a measure of catalytic efficiency with NADPH) is decreased 13.4-fold and 15.5-fold, respectively, compared with wild-type FLDR. By contrast, the k_{cat}/K_m is decreased less than 2-fold for R144A. Despite their apparent similarity in efficiency as NADPH-dependent cytochrome *c* reductases (k_{cat}/K_m, 6.5 ± 0.5 and $5.6 \pm 0.9\ \mu M^{-1} \cdot min^{-1}$, respectively), R174A and R184A exhibit quite different characteristics. Both k_{cat} and K_m values for NADPH-dependent catalysis by R184A are ≈ 2.5-fold greater than the same parameters for R174A (Table 1).

Since the K_m value is a composite parameter and not necessarily a true measure of NAD(P)H affinity, we also analysed the NAD(P)H-dependent reduction of the FAD in FLDR by stopped-flow absorption spectroscopy. Using this technique, we were able to examine the effects of mutations on both the binding of NAD(P)H and the hydride transfer to oxidized FAD, the first two steps in FLDR catalysis. By this method, the binding of NADPH to wild-type FLDR was determined to be very tight (K_d, 5 μM; Table 2), i.e. the flavin-reduction rate was seen to remain constant even when the NADPH concentration was lowered to a level equimolar with that of the FLDR (10 μM). The K_d for NADPH remained very low for mutant R174A ($< 5\ \mu$M). However, the apparent NADPH affinity was much reduced for mutants R144A (K_d, $635 \pm 10\ \mu$M) and R184A (K_d, 2.3 ± 0.06 mM). Despite the apparent high NADPH affinity of R174A, it had the slowest rate of hydride transfer to the FAD. For R174A, the k_{red} was $8.82 \pm 0.52\ s^{-1}$, only 39 % of the wild-type value (Table 2). It is notable also for this mutant that near-UV CD and aromatic amino acid fluorescence properties were altered (Figure 4, right panel, and Figure 5). These features indicate a perturbed tertiary structure in mutant R174A, which may underlie the diminished hydride-transfer rate from NADPH.

Alignment of the amino acid sequence of FLDR with other pyridine dinucleotide-dependent oxidoreductases shows that an

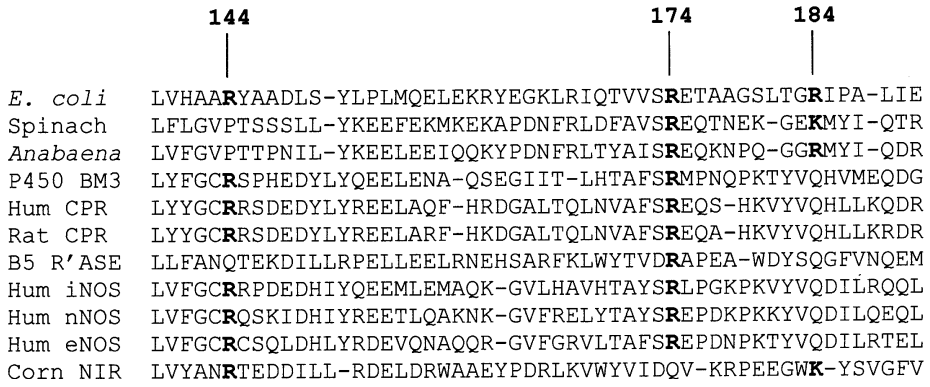

Figure 6 Amino acid alignment of FLDR (from *E. coli*, Swiss-Prot code P28861, [15]) with other members of the FNR family of enzymes

Alignments were performed as described in the Experimental section, comparing other protein sequences with the region of FLDR from L139 to E190 (encompassing all three of the mutated arginines). Flavodoxin reductase arginine residues 144, 174 and 184 are highlighted in bold, as are positively charged amino acids (arginines and lysines) conserved in the aligned enzymes. Spinach, spinach FNR (Swiss-Prot code P00455, [24]); *Anabaena*, ferredoxin reductase from *Anabaena variabilis* (Q4459); P450 BM3, flavocytochrome P450 BM3 from *Bacillus megaterium* (P14779, [25]); Hum CPR, human NADPH–cytochrome P450 reductase (P16435, [26]); Rat CPR, rat NADPH–cytochrome P450 reductase (P00388, [27]); B5 R'ASE, bovine NADH–cytochrome b_5 reductase (P07514, [28]); Hum iNOS, human inducible nitric oxide synthase (NOS; P35228, [29]); Hum nNOS, human neuronal NOS (P29475, [30]); Hum eNOS, human endothelial NOS (P29474, [31]); Corn NIR, corn nitrate reductase (P17571, [32]). Bovine cytochrome b_5 reductase and corn nitrate reductase are NADH-dependent reductases, all other enzymes shown are NADPH-dependent.

arginine corresponding to R174 is strongly conserved in virtually all the $NADP^+$-dependent members of the FNR family (Figure 6). In addition, a serine is also conserved in the majority of related enzymes at a position corresponding to S173 in FLDR. However, the serine is replaced by an acidic residue in many of the NAD^+-dependent members of the FNR family [19]. For instance, in the bovine NADH–cytochrome b_5 reductase, an aspartate replaces the serine. This is also the case in corn nitrate reductase and other related NAD^+-dependent systems [10,13]. By analogy with the NADPH- and NADH-dependent glutathione reductases [20], the aspartate side chains may be involved in hydrogen bonding to the 2′ hydroxy group of the adenosine ribose in NADH, i.e. the functional group that is replaced by phosphate in NADPH. According to their crystallographic studies of the 2′-AMP-bound form of spinach ferredoxin reductase (the 'prototype' enzyme for the FNR family), Karplus et al. [10] identified S234, R235, K244 and Y246 as a cluster of residues whose side chains provide hydrogen bonds to the 2′-phosphate group of bound 2′-phospho-AMP. These residues are predicted to hydrogen-bond to the same position on $NADP^+$ and aid in the discrimination against NAD^+, which has a K_m 400-fold greater than that of $NADP^+$ [21]. The first three of these residues correspond to S173, R174 and R184 in FLDR (a positively charged arginine replaces the lysine at position 184 in FLDR), but an aromatic residue corresponding to Y246 is not conserved in FLDR (Figure 6). By comparison with data for related FNR enzymes, it appears clear that R174 and R184 of FLDR interact with the $NADP^+$ 2′-phosphate group, but that R144 may not. Chemical-modification studies of spinach FNR have also suggested that K116, K244 (equivalent to R184 in FLDR), an unidentified lysine, a carboxylate group and a histidine are involved in $NADP^+$ binding [10].

From the studies of Scrutton et al. [20], mutagenesis of residues analogous to S173 and R174 in FLDR led to alterations in the pyridine nucleotide specificity of glutathione reductase. Several successive mutations were required to achieve a complete conversion of specificity from $NADP^+$ to NAD^+. Multiple mutations will also doubtless be required to convert FLDR to an NADH-dependent reductase. However, if both R174 and R184 are involved in adenosine ribose 2′-phosphate binding (but if R144 is not), then we might expect to observe an increased selectivity for NADH over NADPH in mutants R174A and R184A, but not for R144A. The steady-state and stopped-flow kinetic data presented (Tables 1 and 2) support this theory. In steady-state cytochrome *c* reduction, the k_{cat} for the NADH-dependent reactions for R174A and R184A are 1.3- and 1.5-fold higher than wild-type, respectively, while the k_{cat} for R144A is 2.4-fold lower. The k_{cat}/K_m ratio for NADH-dependent catalysis also indicates that R184A is a more efficient NADH-dependent reductase than wild-type and R144A (Table 1). The comparative efficiency with NADH versus NADPH $[(k_{cat}/K_m)_{NADH}/(k_{cat}/K_m)_{NADPH}]$ for the three mutants indicates that there is partial conversion to NADH preference in R174A and R184A, but not R144A. Stopped-flow studies also indicate that NADH binds more efficiently to R174A and R184A than to R144A (Table 2). The k_{red}/K_d ratio is much higher for R174A and R184A than for R144A. Comparisons of hydride transfer efficiency with NADH versus NADPH $([k_{red}/K_d]_{NADH}/[k_{red}/K_d]_{NADPH})$ based on stopped-flow data indicates that mutant R184A shows a very large alteration in preference towards NADH (> 140-fold) compared with wild-type FLDR.

The kinetic data support the proposal that R174A and R184A are important for binding the adenosine ribose 2′-phosphate of NADPH, although further mutations would clearly be required to convert specificity completely in favour of NADH. The atomic structure of the 2′-phospho-AMP-bound form of spinach FNR indicates that R235 (≡R174 in FLDR) and K244 (≡R184 in FLDR) each probably provide two hydrogen bonds to the 2′-phosphate, but that K116 is also involved in hydrogen bonding to stabilize the adenosine ribose 5′-phosphate group [10]. This lysine is also conserved in FLDR (K83), suggesting that it may play a similar role here. This raises the question as to the specific role of R144 in NADPH interactions in FLDR. An obvious suggestion would be that it is involved in electrostatic interactions or hydrogen bonding with the nicotinamide ribose 5′-phosphate, which is present in both NADH and NADPH. This would explain why, although mutant R144A is profoundly affected in its binding of NADPH and in its catalytic activity towards an artificial electron acceptor (cytochrome *c*), its relative efficiency with NADH is also diminished (not increased, as in R174A and

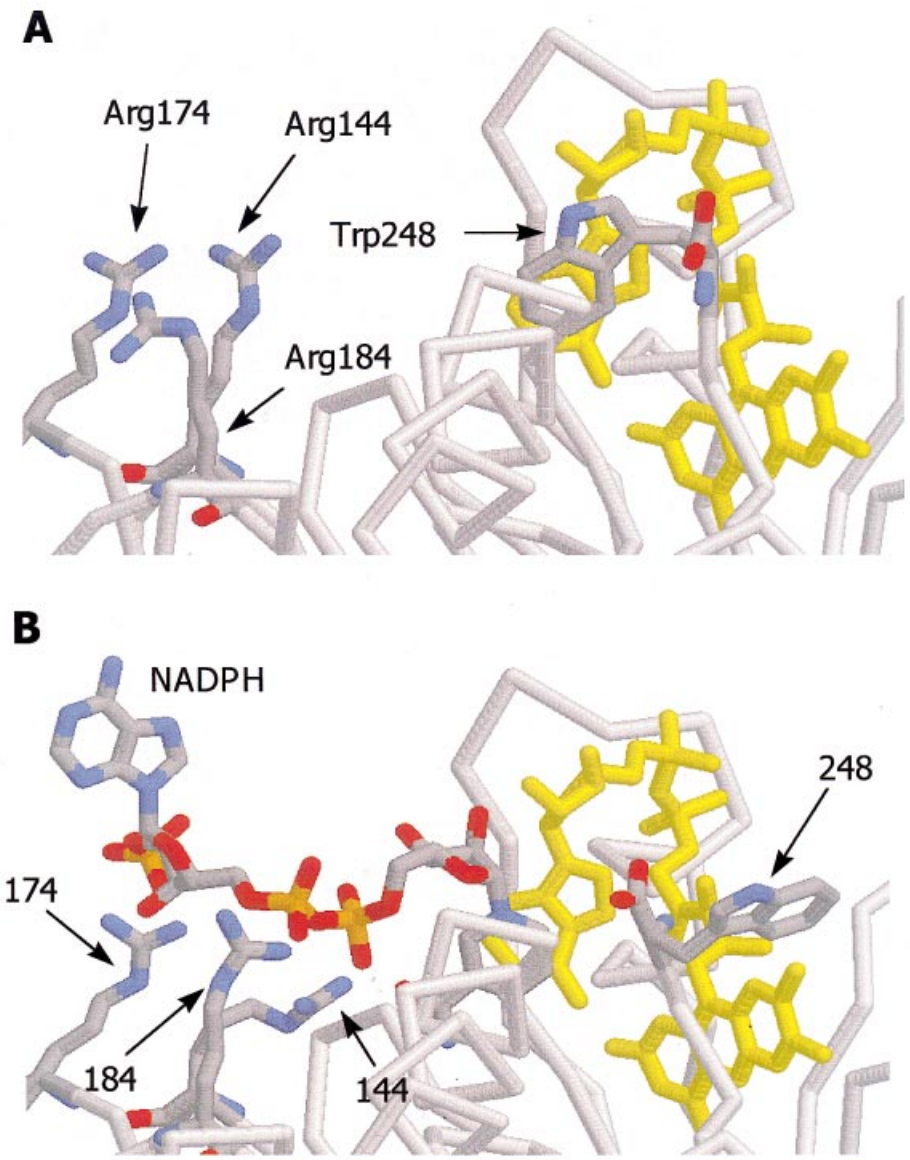

Figure 7 The atomic structure of FLDR and the results of molecular modelling of its interaction with NADPH

Structures are depicted in Rasmol. (**A**) Polypeptide backbone of FLDR (grey) in the region of the proposed NADPH-docking site from the atomic structure of Ingelman et al. [9]. The FAD moiety is yellow, and relevant amino acid side chains (R144, R174, R184 and W248) are also shown, with nitrogen atoms depicted in blue and oxygens in red. Tryptophan-248 obscures access of the nicotinamide ring of NADPH to the flavin in this structure. (**B**) Results of molecular-modelling studies, with NADPH binding optimized. Phosphorus atoms in the docked NADPH are depicted in orange. Tryptophan-248 is rotated away from the adenine moiety of FAD to facilitate closer approach of the NADPH nicotinamide ring, which is now located only 5.8 Å from the FAD isoalloxazine ring system. The arginines are now positioned close enough for potential electrostatic or hydrogen-bonding interactions with the adenosine ribose 2′-phosphate (R174 and R184), adenosine ribose 5′-phosphate (possibly R184) and nicotinamide ribose 5′-phosphate (R144), explaining the deleterious effects of mutating these residues on NADPH-binding and catalytic efficiency.

R184A). An arginine is conserved at a position corresponding to R144 in FLDR in the majority of other $NADP^+$-dependent members of the FNR family, providing further indication for an important role in pyridine nucleotide binding (Figure 6).

To investigate further the binding of NADPH to FLDR, we undertook molecular-modelling studies in attempts to dock the pyridine nucleotide in the FLDR structure close to the FAD, in the binding region identified from the atomic structure of Ingelman et al. [9]. We discovered that the NADPH could not be docked favourably to permit hydride transfer from the nicotinamide ring of NADPH to the FAD, since in the crystal structure of FLDR, the C-terminal amino acid side chain of (tryptophan 248 blocks the entrance to the flavin (Figure 7A). This may explain, at least partly, why the limiting rate of flavin reduction (k_{red}) was only 22.63 s^{-1} for FLDR (Table 2), compared with > 700 s^{-1} for the FAD domain of flavocytochrome P450 BM3, another FNR family member [22,23]. A conformational change to displace W248 on NADPH binding and permit flavin reduction could explain the relatively low rate of hydride transfer measured in FLDR. Molecular modelling was performed with the constraints that the NADPH hydride–FAD isoalloxazine distance should be < 8 Å and that W248 should rotate to expose

the flavin for interaction with NADPH. This modelling resulted in the best-fit docking structure shown in Figure 7(B), where the nicotinamide ring of NADPH approaches the FAD with a minimum distance of 5.8 Å between the two centres. The modelled structure shown in Figure 7(B) also highlights the proximity of the three arginines to the phosphate groups of NADPH. This model indicates that R174 and R184 lie close to the adenosine ribose 2′-phosphate, probably within hydrogen-bonding distance. Interaction between R184 and the adenosine ribose 5′-phosphate may also be feasible. However, R144 is rather more distant from the adenosine ribose, and makes its closest approaches to the nicotinamide ribose 5′-phosphate. The NADPH-bound model structure is consistent with the results from our kinetic studies, placing R174 and R184 much closer to the 2′-phosphate of NADPH (replaced by a hydroxy in NADH) and R144 closer to another phosphate group.

In conclusion, the atomic structure of FLDR implicates the positively charged arginine residues at positions 144, 174 and 184 in the interaction with NADPH. Charge-neutralizing mutations (to alanine) at each of these positions have profound consequences for the efficiency of the mutants to act as NADPH-dependent reductases. The K_m for NADPH and efficiency (k_{cat}/K_m) of cytochrome *c* reduction is diminished in all mutants, with R174A and R184A worst affected. The errors on the K_m values for mutant R144A (5.3 ± 0.7 μM against 3.9 ± 0.3 μM for wild type) indicate that the effect on K_m is only marginal in this case. Whereas R174A maintains a low K_d for NADPH (< 5 μM), the mutation also induces alterations in the near-UV CD and flavin fluorescence spectra, consistent with tertiary structure changes in the vicinity of the NADPH-binding site. Indeed, the fact that the near-UV CD (resulting mainly from aromatic amino acids) is altered suggests that there may be some movement of the tryptophan (W248) that obscures the FAD in the R174A mutant. Molecular-modelling studies of NADPH binding are consistent with the roles of these arginine residues inferred from structural comparisons with other members of the FNR family, and from our kinetic studies. R174 and R184 appear to interact with the adenosine ribose 2′-phosphate, while R144 is more likely to stabilize NADPH binding by interaction with the nicotinamide ribose 5′-phosphate. In particular, mutant R184A shows marked conversion in pyridine nucleotide preference, with the $(k_{cat}/K_m)_{NADH}/(k_{cat}/K_m)_{NADPH}$ ratio for this mutant almost 30-fold greater than for the wild type, and the $K_{d\ (NADH)}/K_{d\ (NADPH)}$ ratio also $>$ 175-fold lower than for the wild type. Our studies have therefore confirmed the importance of these arginine residues in the interaction with NADPH, and have defined distinct roles for these residues in the binding of the coenzyme. In other studies, we are examining the roles of surface-charged residues on FLDR (including arginines 237 and 238), with the aim of understanding better the binding site for FLD, a physiological redox partner for FLDR.

We acknowledge support from the Biotechnology and Biological Sciences Research Council (A.W.M., S.K.C., D.J.C., N.C.P. and S.M.K.). A.W.M. and S.K.C. thank the Royal Society of Edinburgh and Caledonian Research Foundation (Caledonian Research Foundation/Royal Society of Edinburgh Fellowship to A.W.M. and SOEID Fellowship to S.K.C.). A.W.M. and S.K.C. also wish to thank the Leverhulme Trust for the support of their research (postdoctoral assistantship to M.A.N.). C.L. and L.M. are supported by funding from the Edinburgh Centre for Protein Technology and the University of Edinburgh, respectively.

REFERENCES

1 Fujii, K. and Huennekens, F. M. (1974) Activation of methionine synthetase by a reduced triphosphopyridine nucleotide-dependent flavoprotein system. J. Biol. Chem. **249**, 6745–6750

2 Sanyal, I., Cohen, G. and Flint, D. H. (1994) Biotin synthase – purification, characterization as a [2Fe-2S] cluster protein, and *in vitro* activity of the *Escherichia coli bio*B gene product. Biochemistry **33**, 3625–3631

3 Blaschkowski, H. P., Neuer, G., Ludwig-Festl, M. and Knappe, J. (1982) Routes of flavodoxin and ferredoxin reduction in *Escherichia coli* - CoA-acylating pyruvate-, flavodoxin- and NADPH-flavodoxin oxidoreductases participating in the activation of pyruvate formate lyase. Eur. J. Biochem. **123**, 563–569

4 Reichard, P. (1993) The anaerobic ribonucleotide reductase from *Escherichia coli*. J. Biol. Chem. **268**, 8383–8386

5 Bianchi, V., Haggård-Ljungquist, E., Pontis, E. and Reichard, P. (1995) Interruption of the ferredoxin (flavodoxin) $NADP^+$ oxidoreductase gene of *Escherichia coli* does not affect anaerobic growth, but increases sensitivity to paraquat. J. Bacteriol. **177**, 4528–4531

6 Liochev, S. I., Hausladen, A., Beyer, Jr, W. F. and Fridovich, I. (1994) NADPH-ferredoxin oxidoreductase acts as a paraquat diaphorase and is a member of the SoxRS regulon. Proc. Natl. Acad. Sci. U.S.A. **91**, 1328–1331

7 McIver, L., Leadbeater, C., Campopiano, D. J., Baxter, R. L., Daff, S. N., Chapman, S. K. and Munro, A. W. (1998) Characterisation of flavodoxin $NADP^+$ oxidoreductase and flavodoxin; key components of electron transfer in *Escherichia coli*. Eur. J. Biochem. **257**, 577–585

8 Jenkins, C. M. and Waterman, M. R. (1994) Flavodoxin and NADPH-flavodoxin reductase from *Escherichia coli* support bovine cytochrome P450 c17 hydroxylase activities. J. Biol. Chem. **269**, 27401–27408

9 Ingelman, M., Bianchi, V. and Eklund, H. (1997) The three-dimensional structure of flavodoxin reductase from *Escherichia coli* at 1.7 Angstrom resolution. J. Mol. Biol. **268**, 147–157

10 Karplus, P. A., Daniels, M. J. and Herriot, J. R. (1991) Atomic structure of ferredoxin-$NADP^+$ reductase – prototype for a structurally novel flavoenzyme family. Science **251**, 60–66

11 Lu, G., Campbell, W. H., Schneider, G. and Lindqvist, Y. (1994) Crystal structure of the FAD-containing fragment of corn nitrate reductase at 2.5 Angstrom resolution: relationship to other flavoprotein reductases. Structure **2**, 809–821

12 Nishida, H., Inaka, K., Yamanaka, M., Kaida, S., Kobayashi, K. and Miki, K. (1995) Crystal structure of NADH-cytochrome b_5 reductase from pig liver at 2.4 Angstrom resolution. Biochemistry **34**, 2763–2767

13 Correll, C. C., Ludwig, M. L., Burns, C. M. and Karplus, P. A. (1993) Structural prototypes for an extended family of flavoprotein reductases – comparison of phthalate dioxygenase with ferredoxin reductase and ferredoxin. Protein Sci. **2**, 2112–2133

14 Studier, F. W. and Moffat, B. A. (1986) Use of bacteriophage T7 RNA polymerase to direct selective high-level expression of cloned genes. J. Mol. Biol. **189**, 113–130

15 Bianchi, V., Reichard, P., Eliasson, R., Pontis, E., Krook, M., Jornvall, H. and Haggård-Ljungquist, E. (1993) Anaerobic ribonucleotide reduction, cloning of the gene (fpr), and overexpression of the protein. J. Bacteriol. **175**, 1590–1595

16 Yanisch-Perron, C., Vieira, J. and Messing, J. (1985) Improved M13 phage cloning vectors and host strains. Nucleotide sequences of the M13mp18 and pUC19 vectors. Gene **33**, 103–119

17 Sarkar, G. and Sommer, S. S. (1990) The megaprimer method of site-directed mutagenesis. BioTechniques **8**, 404–407

18 Harvey, R. A. (1980) Flavin 1, N^6-ethenoadenine dinucleotide. Methods Enzymol. **66**, 290–294

19 Wierenga, R. K., Terpstra, P. and Hol, W. G. L. (1986) Prediction of the occurrence of the ADP-binding beta-alpha-beta fold in proteins using an amino acid sequence fingerprint. J. Mol. Biol. **187**, 101–107

20 Scrutton, N. S., Berry, A. and Perham, R. N. (1990) Redesign of the coenzyme specificity of a dehydrogenase by protein engineering. Nature (London) **343**, 38–43

21 Shin, M. and Arnon, D. I. (1965) Enzymic mechanisms of pyridine nucleotide reduction in chloroplasts. J. Biol. Chem. **240**, 1405–1414

22 Porter, T. D. (1991) An unusual yet strongly conserved flavoprotein reductase in bacteria and mammals. Trends Biochem. Sci. **16**, 154–158

23 Munro, A. W., Daff, S., Coggins, J. R., Lindsay, J. G. and Chapman, S. K. (1996) Probing electron transfer in flavocytochrome P-450 BM3 and its component domains. Eur. J. Biochem. **239**, 403–409

24 Karplus, P. A., Walsh, K. A. and Herriot, J. R. (1984) Amino acid sequence of spinach ferredoxin $NADP^+$ oxidoreductase. Biochemistry **23**, 6576–6583

25 Ruettinger, R. T., Wen, L.-P. and Fulco, A. J. (1989) Coding nucleotide, 5′ regulatory, and deduced amino acid sequences of P-450 BM-3, a single peptide cytochrome P-450-NADPH-P-450 reductase from *Bacillus megaterium*. J. Biol. Chem. **264**, 10987–10995

26 Haniu, M., McManus, M. E., Birkett, D. J., Lee, T. D. and Shively, J. E. (1989) Structural and functional analysis of NADPH-cytochrome P-450 reductase from human liver. Complete sequence of human enzyme and NADPH-binding sites. Biochemistry **28**, 8639–8645

27 Porter, T. D. and Kasper, C. B. (1985) Coding nucleotide sequence of rat NADPH-cytochrome P-450 oxidoreductase cDNA and identification of flavin-binding domains. Proc. Natl. Acad. Sci. U.S.A. **82**, 973–977
28 Ozols, J., Korza, G., Heinemann, F. S., Hediger, M. A. and Strittmatter, P. (1985) Complete amino acid sequence of steer liver microsomal NADH-cytochrome b_5 reductase. J. Biol. Chem. **260**, 11953–11961
29 Geller, D. A., Lowenstein, C. J., Shapiro, R. A., Nussler, A. K., De Silvio, M., Wang, S. C., Nakayama, D. K., Simmons, R. L., Snyder, S. H. and Billiar, T. R. (1993) Molecular cloning and expression of inducible nitric oxide synthase from human hepatocytes. Proc. Natl. Acad. Sci. U.S.A. **90**, 3491–3495
30 Hall, A. V., Antoniu, H., Wang, Y., Cheung, A. H., Arbus, A. M., Olson, S. L., Lu, W. C., Kau, C. L. and Marsden, P. A. (1994) Structural organization of the human neuronal nitric oxide synthase gene (NOS1). J. Biol. Chem. **269**, 33082–33090
31 Janssens, S. P., Shimoushi, A., Quertermous, T., Bloch, D. B. and Bloch, K. D. (1992) Cloning and expression of a cDNA encoding human endothelium-derived relaxing factor nitric oxide synthase. J. Biol. Chem. **267**, 14519–14522
32 Gowri, G. and Campbell, W. H. (1989) cDNA clones for corn leaf NADH-nitrate reductase and chloroplast $NADP^+$-glyceraldehyde-3-phosphate dehydrogenase. Characterization of the clones and analysis of the expression of the genes in leaves as influenced by nitrate in the light and dark. Plant Physiol. **90**, 792–798

Received 24 March 2000/12 September 2000; accepted 28 September 2000